Journal of Catalysis **183,** 91–101 (1999)
Article ID jcat.1998.2368, available online at http://www.idealibrary.com on IDEAL®

Adsorption-Induced Structural Changes of Rh Supported by $TiO_2(110)$-(1×2): An STM Study

A. Berkó and F. Solymosi

Institute of Solid State and Radiochemistry, A. József University, and Reaction Kinetics Research Group, Hungarian Academy of Sciences,[1] *P.O. Box 168, H-6701 Szeged, Hungary*

Received September 18, 1998; accepted November 14, 1998

Effects of different gases (CO, NO, H_2, CO_2) on the morphological changes of Rh nanoparticles deposited on $TiO_2(110)$-(1×2) surface were studied by scanning tunneling microscopy. The planar model catalyst surface was prepared by evaporation of Rh on TiO_2 at room temperature followed by annealing in UHV. By the variation of the Rh content and the annealing temperature Rh nanoparticles can be produced in the range of 1–10 nm. A very rapid disintegration of the supported Rh nanoparticles of 1–2 nm to atomically dispersed Rh was observed at 300 K even after a few minutes exposure to a pressure of 10^{-1} mbar CO. For particle sizes of 3–4 nm the CO-induced process became slower, and for larger Rh clusters (8–10 nm) it did not occur at all even at higher CO pressure. Keeping the atomically dispersed Rh in CO above 500 K led to the reformation of the Rh clusters but of larger size. The CO-induced agglomeration was also observed for larger Rh particles (5–6 nm) above 500 K. The adsorption of NO on Rh nanoparticles also resulted in the disruption of Rh_x crystallites at 300 K. It was not observed, however, in the presence of H_2 and CO_2, which was explained by the different nature of their interaction with Rh. © 1999 Academic Press

1. INTRODUCTION

An interesting, but not fully explored feature of the chemistry of some nanostructured materials is that their size and morphology can be strongly influenced by an interaction with reacting gases which may lead to basic changes of their adsorptive and catalytic performances (1, 2). In heterogeneous catalysis it is a well-known phenomenon that the state and the structure of catalyst can be basically altered during the catalytic reaction, and in many cases the real catalyst is formed on the effect of reacting system. MoO_3/ ZSM-5 catalyst provides an excellent example of this phenomenon. As a result of the high-temperature interaction with methane, MoO_3 is transformed into Mo_2C, which is the key compound in the conversion of methane into benzene in this catalyst system (3, 4). Recent studies, however, revealed that structural changes of the catalyst may occur not only during high-temperature reaction, but even during low-temperature adsorption. From the analysis of EXAFS, IR, XPS, and SPA-LEED results it was inferred that the adsorption of CO at 150–400 K caused the disruption of Rh nanoparticles to isolated Rh atoms which may be oxidized to Rh^1 by the OH groups of the support (5–13). As the disruption of Rh_x can also occur on a hydroxyl-free substrate, a stabilization of the atomically dispersed Rh by oxygen vacancies was also suggested (14, 15). At higher temperatures, above 423 K, CO induced the reverse process, e.g., the reductive agglomeration of Rh^1 species into Rh_x clusters (7, 12, 13, 16–19). As regards other systems, there is strong IR and EXAFS evidence that similar processes occur following CO adsorption on supported Ru (20–22), Ir (23), and Re (24–26).

In the present paper we apply scanning tunneling microscopy (STM) to observe directly the adsorption-induced changes of the sizes and morphology of Rh nanoparticles supported on the $TiO_2(110)$-(1×2) surface. The first STM evidence for the CO-induced disruption of supported Rh was reported in our preliminary study (27). The STM technique was subsequently applied in following the disintegration and agglomeration of Ir nanoparticles on $TiO_2(110)$ surface caused by CO (28).

The primary aims of this work are to explore the effect of the size of the Rh particles on the CO-induced processes and to examine the influences of other gases on the state of Rh crystallites. Particular attention is paid to the effect of NO which—according to IR studies—markedly promotes the CO-induced disintegration of supported Rh (29–33).

As a support, we choose a $TiO_2(110)$-(1×2) single crystal which—due to its semiconducting properties—is more suitable for STM studies than other oxidic supports. The main structural features of clean TiO_2 single crystal surfaces, revealed by STM, have already been reported (34–40). The $Rh/TiO_2(001)$ and (110) systems have been characterized by STM as well (41–44).

[1] This laboratory is a part of the Center for Catalysis, Surface and Material Science at the University of Szeged.

0021-9517/99 $30.00
Copyright © 1999 by Academic Press
All rights of reproduction in any form reserved.

2. EXPERIMENTAL

The experiments were performed in a UHV chamber equipped with a three-grid AES-LEED analyzer and a commercial STM head (WA-Technology). The sample can be moved by a UHV-compatible transfer system from the STM head to the central manipulator for annealing in UHV, sputtering by Ar^+, and AES-LEED detection. A side vacuum chamber connected to the main system served for high-pressure gas treatment of the probe at different temperatures. Both chambers were iongetter-pumped. A titanium sublimation pump was also applied in order to increase the pumping speed and to arrive at an ultimate pressure of 5×10^{-8} Pa.

The polished TiO_2(110) single crystal sample was purchased from Crystal-Tec. It was clipped with a Ta plate connected to a transferable sample holder and moved into the UHV chamber. The sample was heated by a W filament positioned just below the Ta plate holding the probe. By this arrangement we could attain a surface temperature of 1100 K measured by a thin chromel–alumel thermocouple attached to the edge of the sample.

The cleaning procedure of the TiO_2 surface started with a few hours annealing at 800 K in an UHV environment. During this treatment the light blue transparent color of the sample became dark grey and opaque as a result of partial reduction. Further cleaning of the surface consisted of cycles of Ar ion bombardment (1.5 keV) for 10 min at room temperature or at 1000 K, and annealing for 1 h at 1100 K. Heating and cooling rates were always less than 2 K s^{-1}. From time to time the crystal was reoxidized in 10^{-4} Pa oxygen at 800 K. This latter treatment radically reduced the corrugation of the surface and resulted in good quality large (110) terraces. Before Rh deposition, the TiO_2 sample was annealed at 1100 K for 10 min.

The homemade evaporator was a liquid nitrogen-cooled device with ohmically heated Rh filament. During the Rh dosing the distance between the evaporator source and the sample was approximately 20 mm. The rate of the deposition was controlled by adjusting the filament current. Auger spectra registered at different points of the sample revealed a uniform and clean rhodium overlayer. The Rh coverage is expressed in monolayer equivalent (ML) which corresponds to 1.6×10^{15} atom/cm^2. The detailed calibration procedure was described in (42, 43). High-purity gases of H_2, CO, CO_2, and NO were introduced into the transfer chamber for gas exposure.

For STM imaging the chemically edged W tip was sharpened *in situ* above the TiO_2 surface by applying 5–10 V pulses, or by using a continuous positive 40–70 V bias potential and 100 nA current (between the tip and the sample in tunneling position) for a few minutes. The inefficiency of this procedure indicates that the tip needs to be changed. Tunneling conditions of +1.5 V bias voltage and 0.2 nA tunneling current were typically used for STM imaging. It is worth mentioning that in the case of gas-exposed surfaces the tunneling current was usually reduced to 0.02 nA and the scan speed also was lowered to some extent in order to receive better quality STM images. We assumed that the higher tunneling current may induce some desorption of the adsorbed molecules, thus hindering a good quality imaging.

3. RESULTS AND DISCUSSION

3.1. Growth of Rh Particles in Vacuum

Figure 1 shows the main features of the Rh/TiO_2(110)-(1×2) system with different Rh contents. The deposition of approximately 0.01 ML of Rh at room temperature results in highly dispersed round-shaped, approximately 1.5-nm-diameter metal particles consisting of 5–6 atoms. The original 1×2 reconstruction of the titania does not undergo any changes even in the region close to the crystallites. Rh clusters are mainly located on the terraces (no step decoration). By increasing the rhodium coverage up to 0.2 ML, the average particle size increases from 1.5 to 3.0 nm, accompanied by a concealing of the original row structure characteristic for the (1×2) reconstruction of TiO_2(110). The aspect ratio of height/diameter of the 3D Rh nanoparticles was approximately 0.3 in the total coverage range. The overall bumpy morphology of the surface remains unchanged in the Rh coverage of 0.1–1.0 ML. It is not yet clear whether this behaviour is connected to a stronger interaction between the Rh overlayer and the titania support (i.e., Rh-induced reduction of TiO_2 phase), or the bumps simply consist of rhodium. The earlier photoelectron spectroscopic results do not support a stronger interaction (oxidation reduction cycle) between Rh and titania at room temperature (45).

In Fig. 1 we also display the effects of annealing of Rh/TiO_2(110)-(1×2) on the shape and the size of the Rh crystallites. At the lowest Rh content (0.01 ML; the average size of Rh is 1.5 nm), a slight increase occurred in its size during annealing—it became 2.5 nm at 500 K, 3.0 nm at 700 K, and 3.5 nm at 900 K. At 0.2 ML, the size of the Rh particles increased from 3.0 nm (300 K) to 4.5 nm following annealing at 900 K. The extent of the size growth was practically the same in the range of 3–5 nm for 0.92 ML Rh coverage. We note that for Rh coverages higher than 0.1 ML, a clear structural separation of Rh nanocrystallites from the (1×2) ordered substrate occurs only after annealing at 1100 K (44).

3.2. Effect of CO

Before the study of the influence of CO on the morphology of Rh crystallites, some measurements were performed with pure, Rh-free TiO_2(110)-(1×2). The exposure of clean titania to CO (approximately 10^8 L) at room temperature exerted only a very slight influence on the surface structure, although small protrusions appear on the surface

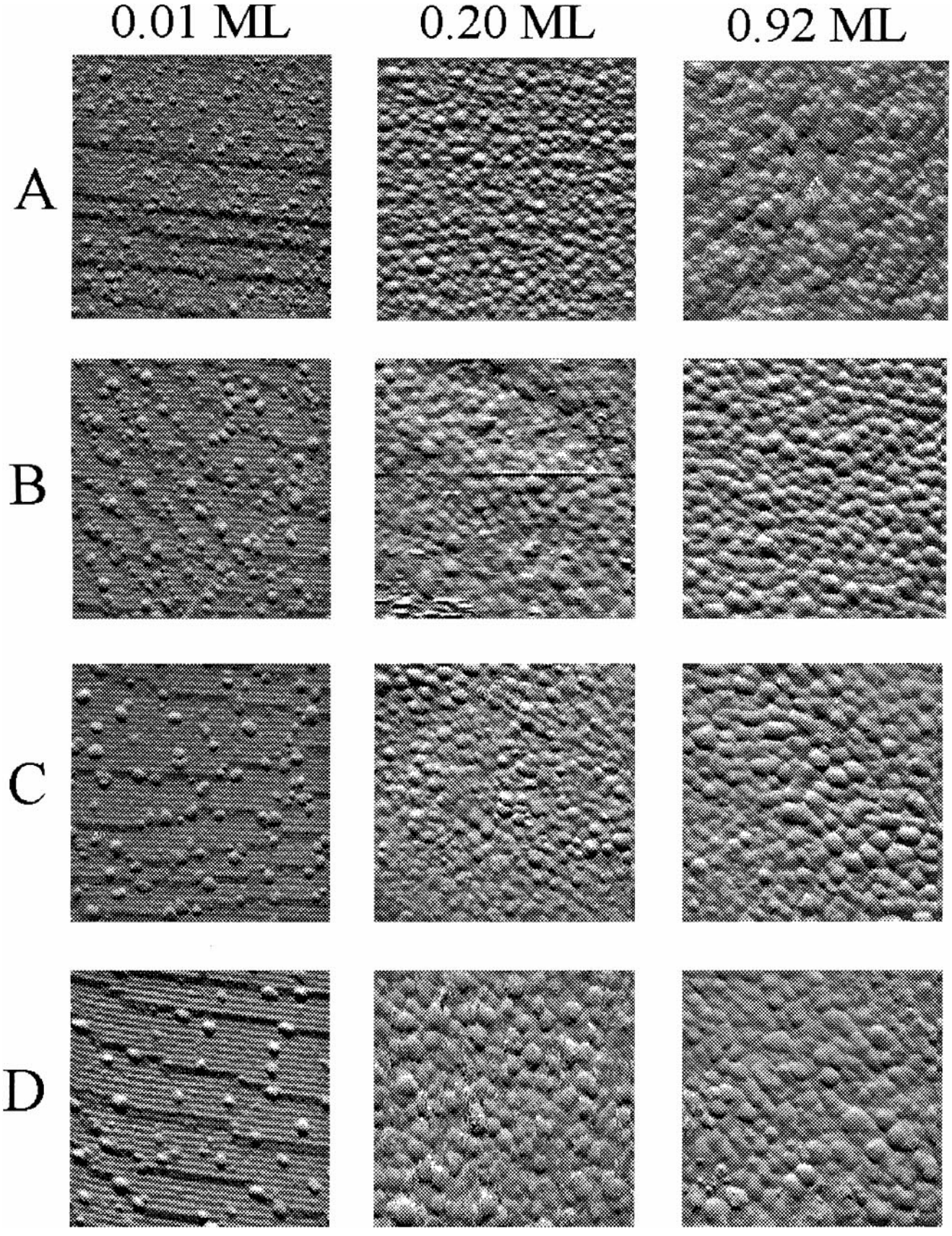

FIG. 1. Effects of annealing on the STM images (50 nm × 50 nm) of $Rh/TiO_2(110) - (1 \times 2)$ at different Rh contents (Θ_{Rh}). (A) 300 K; (B) 500 K; (C) 700 K; (D) 900 K.

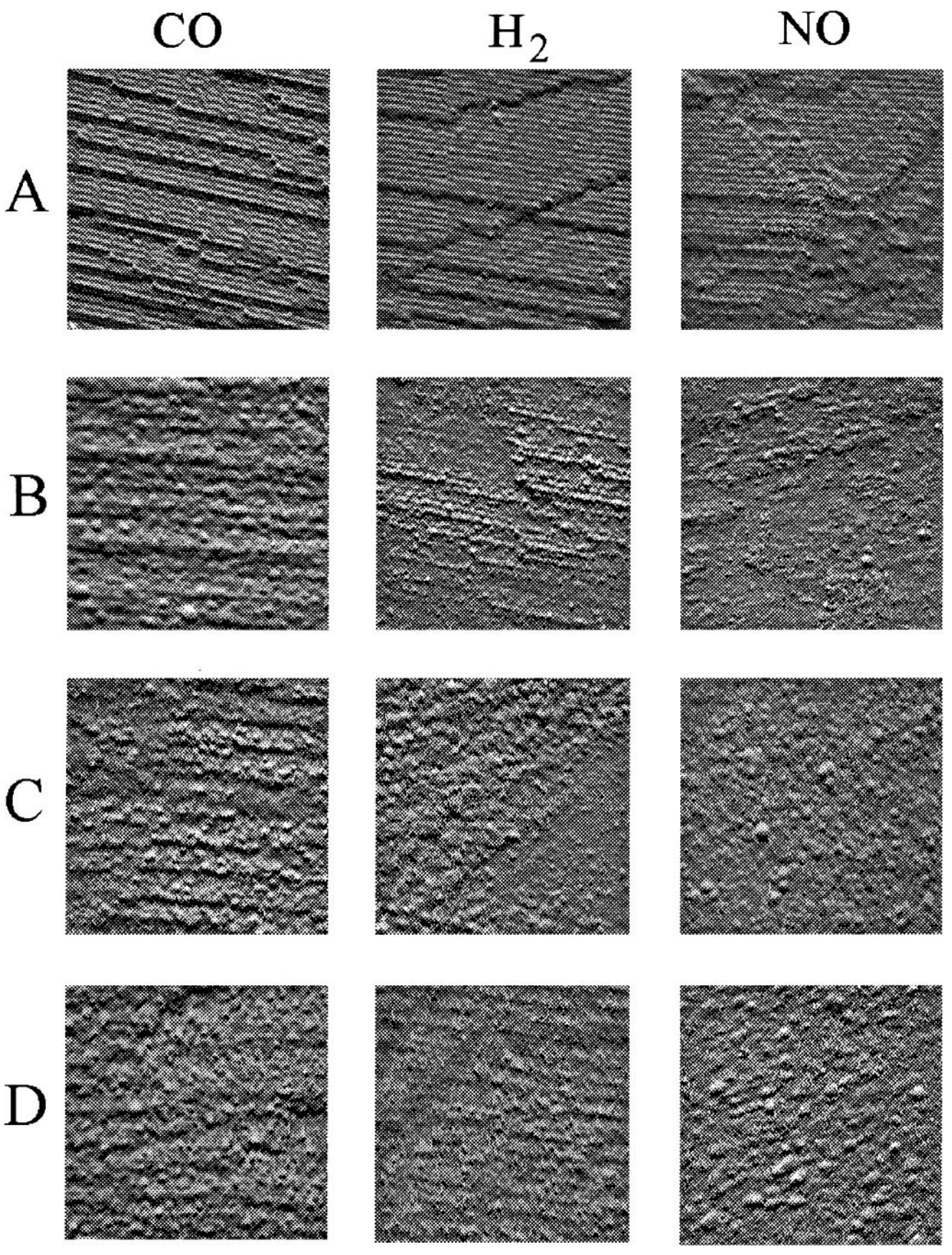

FIG. 2. Effects of the adsorption of CO, H_2, and NO on the STM images (50 nm × 50 nm) of TiO_2 at 300 K. (A) Clean TiO_2; (B) 1×10^{-3} mbar gas at 300 K; (C) 1×10^{-1} mbar at 300 K; (D) 1×10^{-1} mbar at 400 K. Exposure time: 10 min.

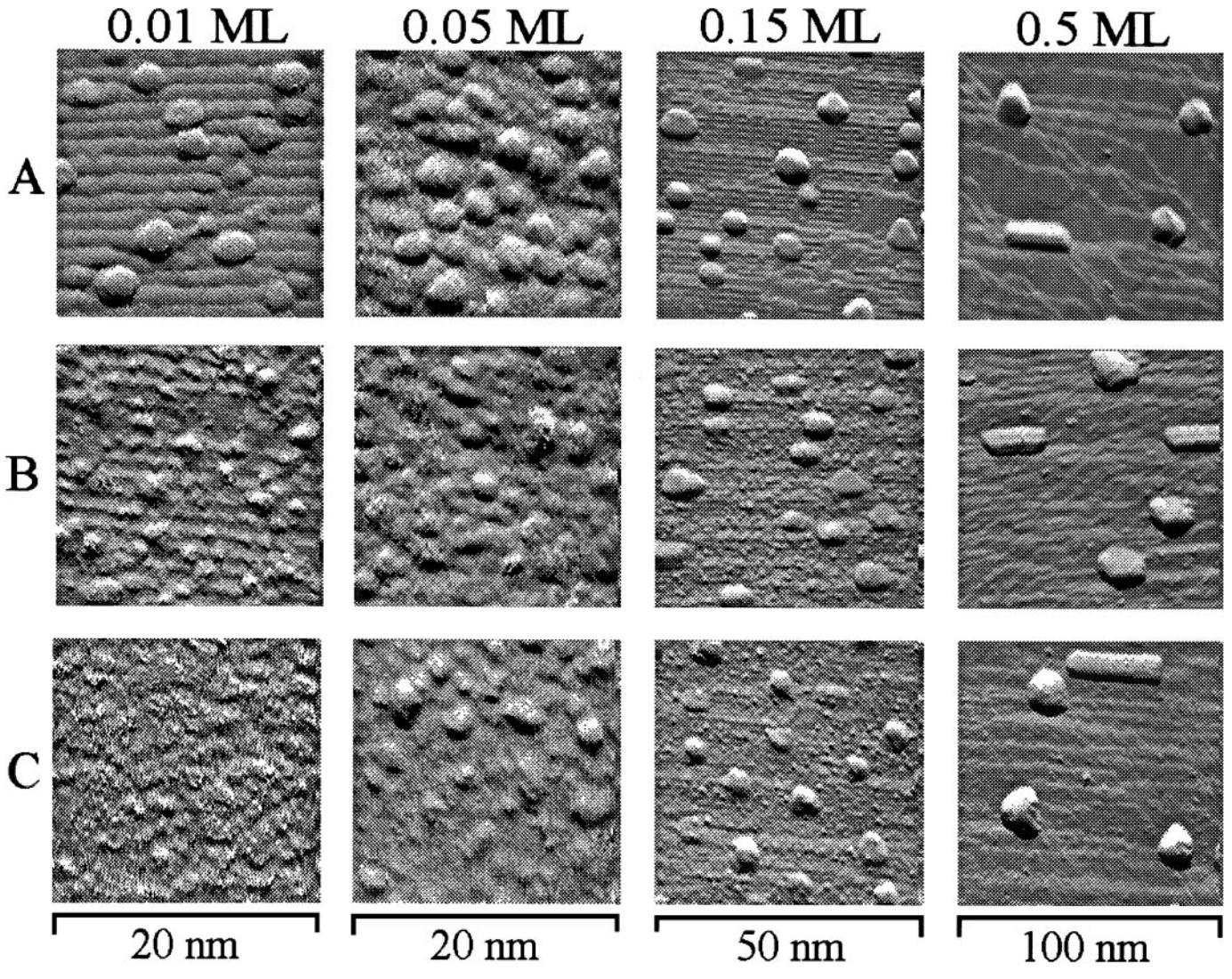

FIG. 3. Effects of CO adsorption at 300 K on $Rh/TiO_2(110)$-(1×2) at different (average) particle sizes. (A) Before CO adsorption. After exposures to CO (B) 10^{-3} mbar, (C) 10^{-1} mbar. Exposure time: 10 min. Note the different scales of the images.

(Figs. 2A–2C). The sharpness of the terrace and row structure of the clean titania decreased at 300 K and disappeared at 400 K (Fig. 2D).

Following the adsorption of CO on Rh/TiO_2 at 0.01 ML of Rh, the size of the Rh crystallites (~1.5 nm) clearly decreased even in the presence of 10^{-3} mbar of CO (Fig. 3). At higher CO pressure, the effect is more dramatic: the Rh particles are hardly detectable by STM. When the coverage of Rh was increased to 0.05 ML, similar phenomena were observed, but the CO-induced change occurred somewhat slower (Fig. 3). Note that in this case the size of the particles was only slightly larger, but the density of the particles was markedly higher. In the next experiments the Rh coverage was increased to 0.15 ML. In order to obtain well separated Rh particles of 3–4 nm, the sample was annealed in UHV at 1100 K. In this case the main process was the corrosion of the particles, but a reduction in their sizes can also be observed. A completely different behaviour was observed for larger Rh particles (8–10 nm), where no changes in size and morphology of the Rh clusters were experienced at 300–400 K even after extended adsorption time, and at higher CO pressure, up to 10 mbar (Fig. 3).

In subsequent measurements, the Rh/TiO_2 samples treated with CO at room temperature have been heated to higher temperature in the presence of CO (1×10^{-1} mbar). Changes in the shape and the size of Rh are shown in Fig. 4. In the case of 0.01 ML of Rh, the round forms attributed to Rh_x crystallites appeared again already at 400 K and became more appreciable at higher temperatures. The average diameter of the Rh_x clusters attained a value of 5.5 nm after the treatment in CO at 600 K. A similar feature was observed at higher Rh contents (0.28 and 1.26 ML).

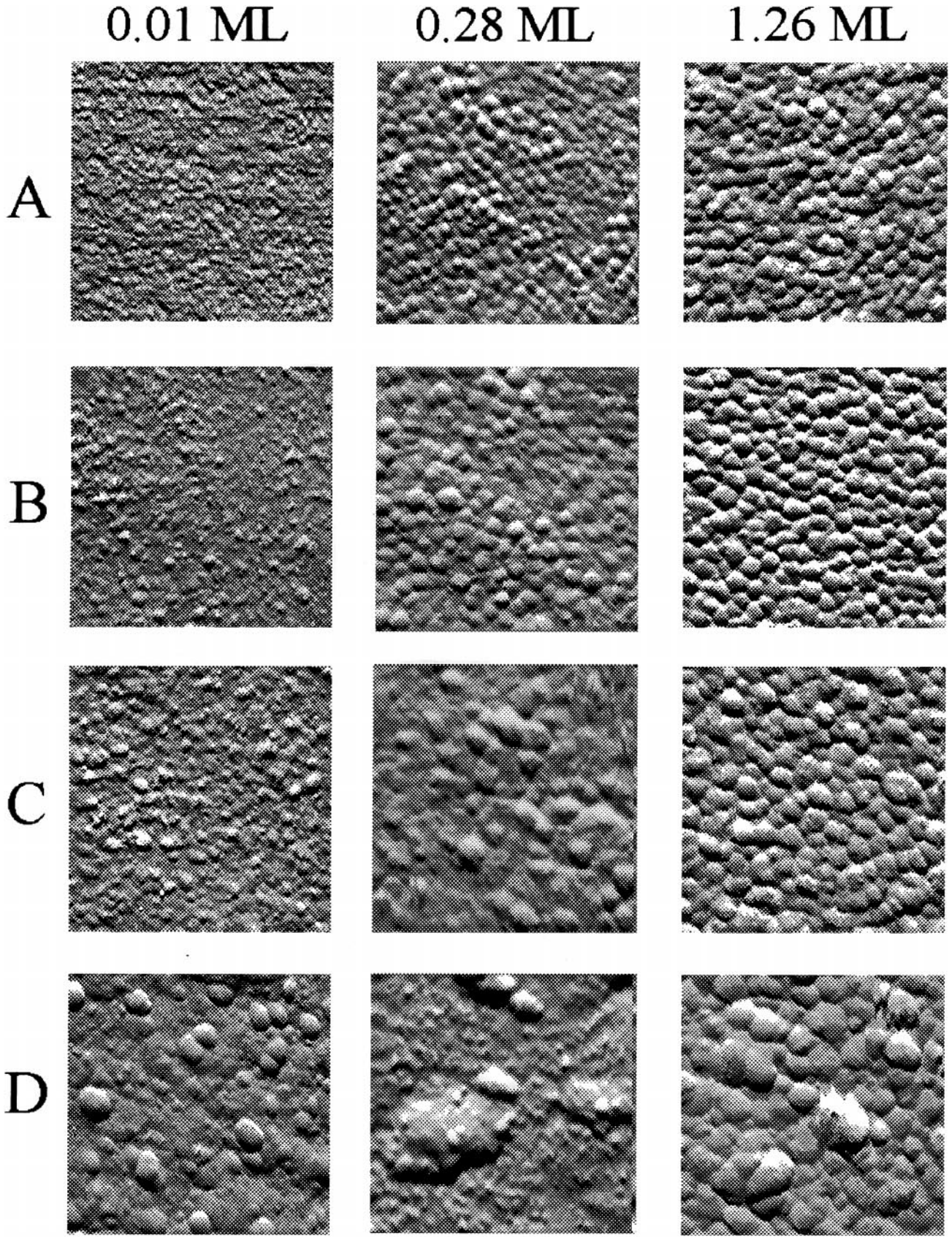

FIG. 4. STM images (50 nm × 50 nm) of $Rh/TiO_2(110)$-(1×2) at different Θ_{Rh} (deposition of Rh was performed at room temperature) following 1×10^{-1} mbar CO adsorption for 10 min at different temperatures. (A) 300 K; (B) 400 K; (C) 500 K; (D) 600 K.

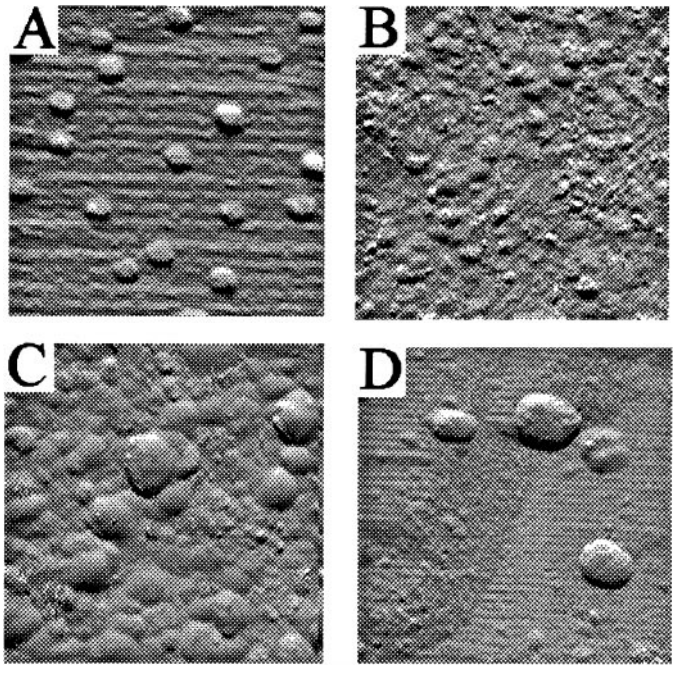

FIG. 5. STM images (50 nm × 50 nm) of $Rh/TiO_2(110)$-(1×2) following CO adsorption at different temperatures. Titania was exposed to 0.10 ML of Rh at room temperature and annealed for 10 min at 1100 K in UHV. (A) Before CO treatment, and after treatments in 1×10^{-1} mbar CO at (B) 300 K and (C) 600 K. (D) The same surface after annealing in UHV for 10 min at 1100 K.

Although the nanoparticles were not disrupted by CO previously at 300–400 K in this case, the adsorption of CO at higher temperature also caused an increase in the size of the Rh crystallites. The extent of size increase was 3–4 times larger than observed in vacuum.

The same results were obtained for the $Rh/TiO_2(110)$-(1×2) surface annealed at 1100 K in UHV and treated with CO at 300 K to obtain disrupted Rh crystallites (Fig. 5). In this case the CO-induced growth of disintegrated particles occured at 600 K (Fig. 5C). The Rh crystallites reappeared much larger than before CO adsorption (Fig. 5C). The particle size, however, did not increase further when the CO-treated surface was subsequently annealed in UHV at 1100 K (Fig. 5D).

These results provide direct evidence for the conclusions drawn from previous EXAFS (5, 6) and IR spectroscopic studies (7–12, 16–18). The small Rh crystallites (1–2 nm) are readily disrupted by CO adsorption, whereas such a process is much slower for particles of 3–5 nm size or cannot be observed for Rh clusters larger than 8–10 nm. The driving force behind this process is very likely the high bond energy of Rh–CO (185 kJ/mol) compared to that of the Rh–Rh bond (532/12 = 44.5 kJ/mol (5)). Note that after extended adsorption time, 10–20 h, the formation of Rh dicarbonyl species, indicative of the occurrence of the disruption, has been detected by means of sensitive FTIR spectroscopy even for larger Rh clusters (7). However, the extent of the disruption of Rh crystallites was extremely low.

The CO-induced agglomeration at elevated temperatures (above 500 K) observed by IR spectroscopy (7, 16–18) has been confirmed by the present STM measurements as well. This was not restricted to isolated Rh atoms, but occurred for larger Rh particles, too. We may assume that the transient formation of $Rh(CO)_2$ moieties also plays a role in the CO-promoted agglomeration of Rh clusters. This is followed by the diffusion of these species—which may occur more easily than that of Rh metal particles—then by the decomposition of $Rh(CO)_2$.

It is important to note that the temperature at which the agglomeration starts (approximately 500 K) is nearly the same as the temperature of CO desorption from extended Rh surfaces. In other words, the frequency of the

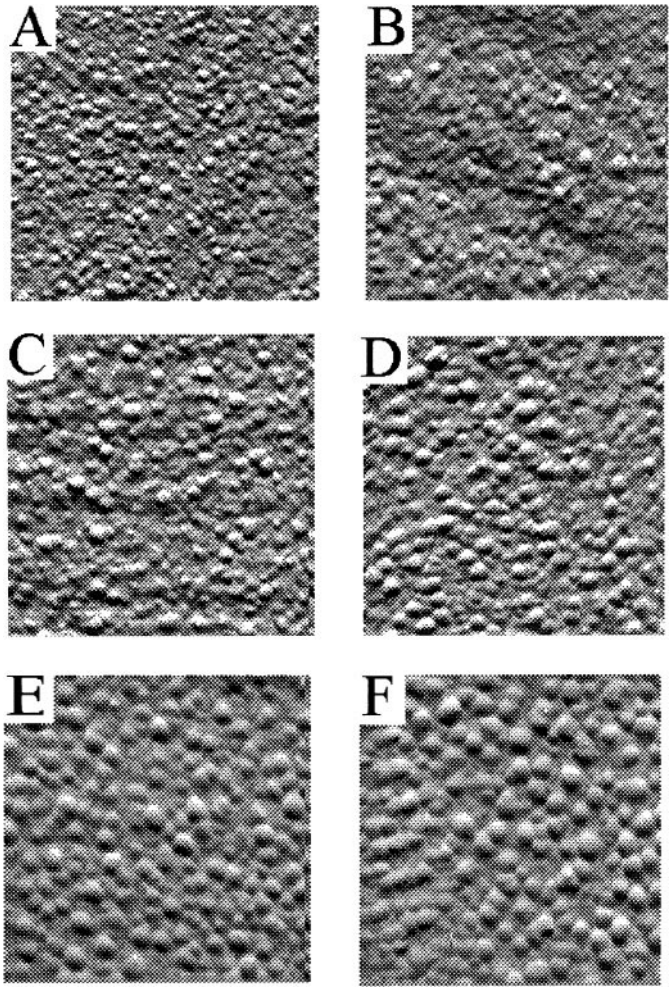

FIG. 6. Effects of H_2 exposure on the STM images (50 nm × 50 nm) of $Rh/TiO_2(110)$-(1×2) ($\Theta_{Rh} = 0.02$). (A) Before H_2 adsorption; (B) 1×10^{-3} mbar H_2 at 300 K; (C) 1×10^{-1} mbar H_2 at 300 K, (D) at 400 K, (E) at 500 K, and (F) at 600 K. Exposure time: 10 min.

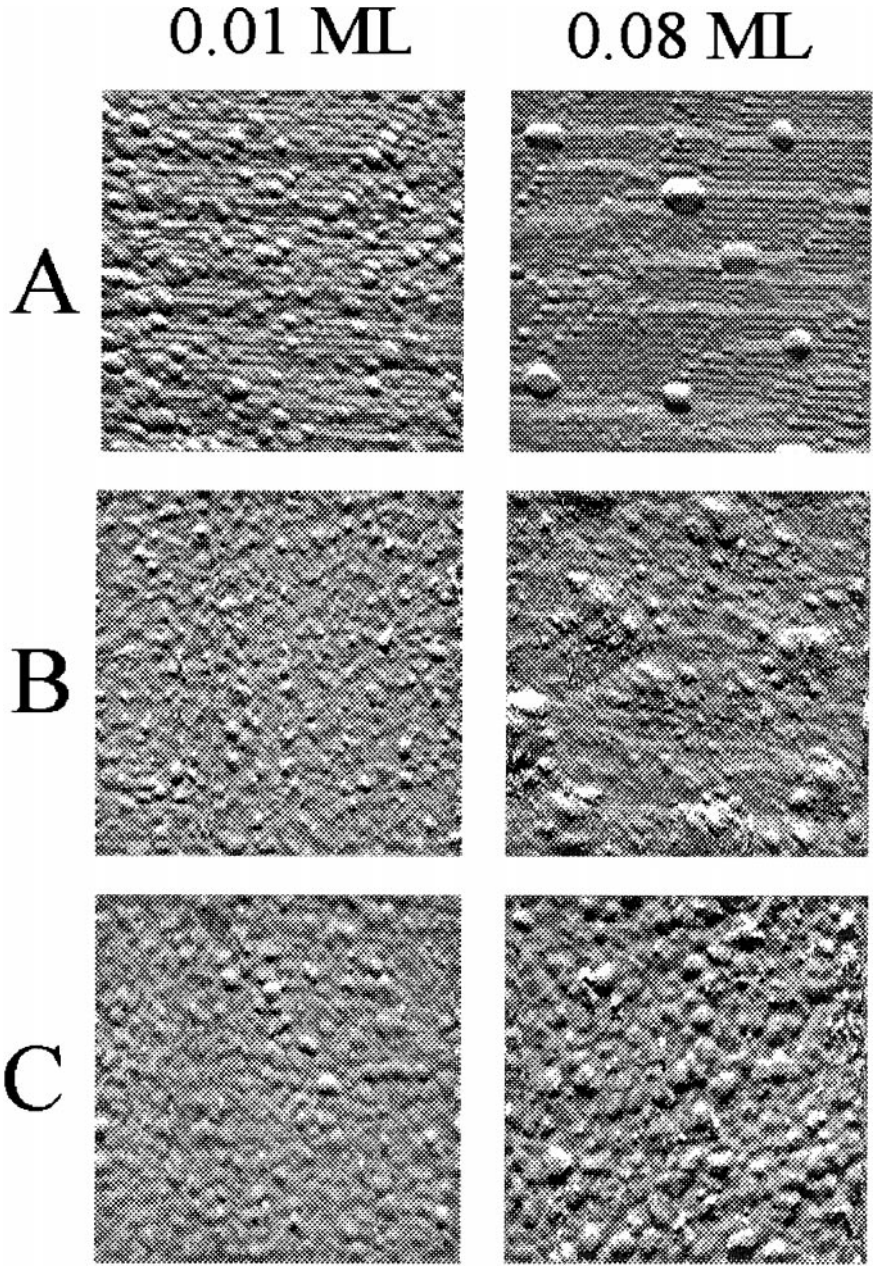

FIG. 7. Effects of NO exposure on the STM images (50 nm × 50 nm) of $Rh/TiO_2(110)$-(1×2) at 300 K at Rh coverages of 0.01 and 0.08 ML. (A) before NO adsorption; (B) 1×10^{-3} mbar NO; (C) 1×10^{-1} mbar NO. Exposure time: 10 min.

adsorption–desorption processes is very high around this temperature.

3.3. Effect of Hydrogen

Exposing the Rh-free titania surface to 10^{-3} mbar H_2 for 10 min the row structure looses its sharpness, similarly as observed following CO adsorption (Fig. 2). An increase of the H_2 pressure to 1×10^{-1} mbar causes a total destruction of the row structure. Annealing the titania in the presence of H_2 at 400 and 500 K results in a further erosion of the surface structure, but it does not lead to a strong structural change, which would prevent the study of the interaction between hydrogen and rhodium.

Although the adsorption of hydrogen on supported Rh has been the subject of several studies, no information is available regarding whether hydrogen can induce similar disruption processes as observed for CO. In this case, IR spectroscopy cannot be used to establish any structural changes; thus a more powerful method, like STM, is required for this purpose.

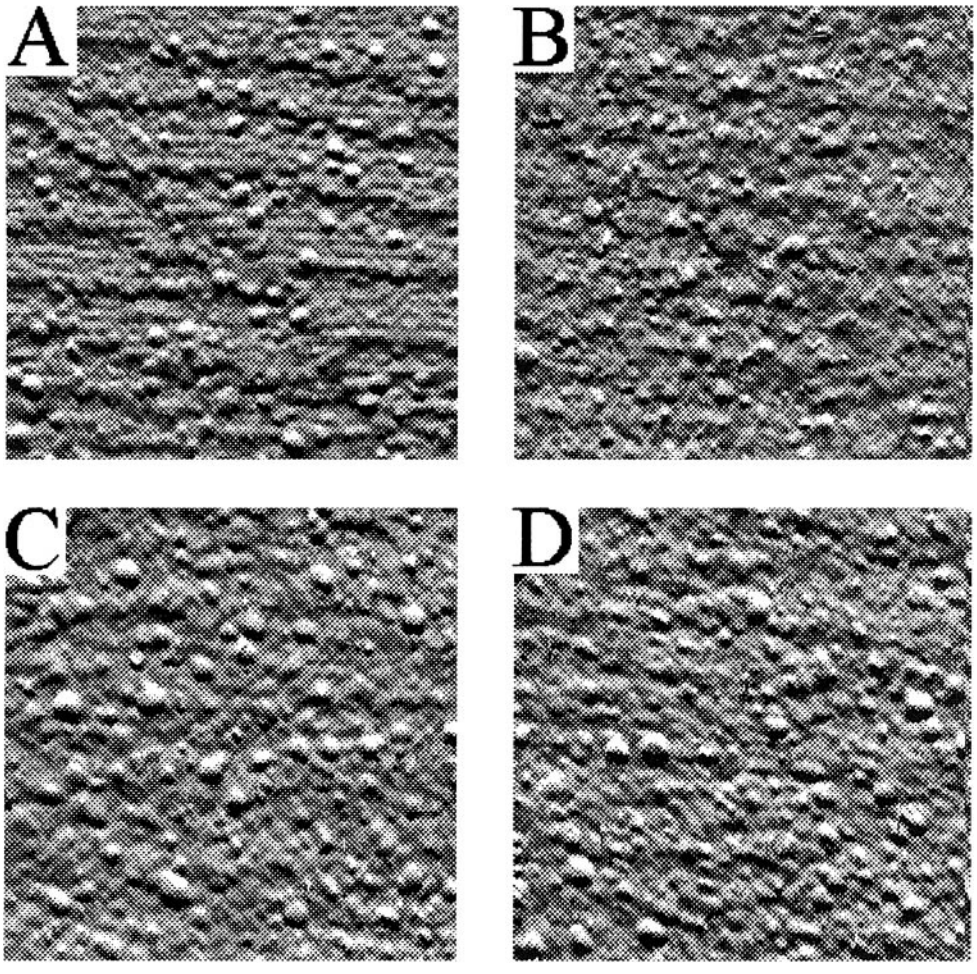

FIG. 8. Effects of CO_2 exposure on the STM images (50 nm × 50 nm) of $Rh/TiO_2(110)1 \times 2$ at 300 K ($\Theta_R = 0.01$). (A) Before CO_2 adsorption; after CO_2 exposure of (B) 1×10^{-1} mbar, 10 min; (C) 10 mbar, 10 min; (D) 10 mbar, 60 h.

Exposing the $Rh/TiO_2(110)$ to H_2 at 300 K caused practically no change in the morphology and size of Rh_x cluster independently of the size of the Rh (Fig. 6). A slight increase in the size of Rh occurred at 500 K from 2.0 to 2.5 nm, and a further increase occurred at 600 K (to 3.0 nm). It is important to point out that this increase in the size of the Rh_x is much less compared to the effect of CO at the same temperature.

Accordingly, independently of the size of the Rh crystallites, the adsorption of hydrogen does not induce a disintegration of Rh nanoparticles. This is possibly due to the fact that the bond energy of Rh–H is smaller (110 kJ/mol) than that of Rh–CO, and thus the formation of the Rh–H bond is not sufficient to induce the rupture of the Rh–Rh bond. Another factor is that in the case of CO adsorption the isolated Rh atoms are oxidized to Rh^1, very likely by the OH groups of the support (7, 9), and the Rh^1 thus produced is stabilized in the form of $Rh^1(CO)_2$. Such a way of stabilizing isolated Rh atoms does not exist in the case of adsorbed hydrogen. At higher temperatures, however, as the STM pictures reveal, the hydrogen leads to an increase in the size of Rh nanoparticles, in accord with the known agglomerizing effect of hydrogen. Note that adding hydrogen to CO in larger quantities prevented the CO-induced disruption of Rh_x clusters even at 300 K, which was attributed to the reducing effect of hydrogen and to the destruction of the $Rh^1(CO)_2$ complex (8).

3.4. Effect of NO

The adsorption of NO on pure $TiO_2(110)$-(1×2) corroded its surface more extensively than that of CO or H_2. The row structure disappeared even at 300 K, as illustrated in Fig. 2. At 400 K, and particularly at 500 K (not shown here), a large-scale hilly structure appeared which was accompanied by a drastic increase of the overall corrugation of the surface. This feature makes it somewhat difficult to determine the effect of NO adsorption on the morphology of Rh_x cluster at higher temperatures.

As shown in Fig. 7, the adsorption of NO on $Rh/TiO_2(110)$-(1×2) at 0.01 ML clearly diminished the size of the 2.0 nm Rh clusters and even caused the disappearance of the round-shaped structure at 300 K. When the Rh content was increased (0.08 ML) and the sample was annealed at 1100 K in UHV, which caused a growth of the size of Rh to 4 nm, similar features were observed. No, or only a very slight, alteration in the STM images was observed for Rh particles larger than 6–8 nm.

These results provided evidence for our previous assumption that the adsorption of NO can also induce the disruption of Rh particles (29). The effect of NO can be explained in the same way as that of CO. As NO adsorbs more strongly on Rh than CO (46), it is not surprising that it causes a similar phenomenon. As was established by IR studies, NO also forms a surface complex, $Rh^1(NO)_2$, with isolated Rh atoms or ions (29–31), and so a stabilizing possibility may exist for these highly reactive Rh atoms.

3.5. Effect of CO_2

Although CO_2 adsorbs readily on the TiO_2 surface forming surface carbonate species, we did not experience radical structural changes by STM for the clean $TiO_2(110)$-(1×2) surface. The adsorption of CO_2 or Rh/TiO_2 containing 0.01 ML of Rh caused no observable changes in the size and shape of the Rh nanoparticles (Fig. 8). The more or less well separated Rh nanocrystallites of $\sim$2.0 nm are well detectable even after 60 h exposure to 10 mbar CO_2 (Fig. 8D). These features are consistent with the very weak interaction between Rh and CO_2 (47–49). Following the adsorption of CO_2 on H-free Rh(111) or on supported Rh at and above 300 K produced no spectral features attributable to adsorbed CO_2 (49).

CONCLUSIONS

(i) STM measurements provided direct evidence for the CO-induced structural changes of Rh nanoparticles. At lower temperatures, 300–400 K, the disruption of Rh crystallites to smaller units and/or to atomically dispersed Rh is the dominant reaction, whereas at higher temperature CO induces the agglomeration of finely dispersed Rh into larger crsytallites. (ii) The disruption process sensitively depends on the size of the Rh nanoparticles: small particles are disrupted easily, whereas the disruption is much slower or did not occur at all for larger nanocrystals. (iii) Adsorption of strongly adsorbed NO also causes the desintegration of small nanoparticles. (iv) In contrast, no structural changes of Rh nanoparticles were experienced in the presence of H_2 and CO_2 even at higher gas pressure.

ACKNOWLEDGMENT

This work was supported by the Hungarian Academy of Sciences and by OTKA 14889.

REFERENCES

1. Fendler, J. H., and Meldrum, F. C., *Adv. Mater.* **7**, 607 (1995).
2. Fendler, J. H., and Dékány, I. (Eds.), "Nanoparticles in Solids and Solution." Kluwer Academic, Dordrecht/Norwell, MA, 1996.
3. Wang, D., Lunsford, J. H., and Rosynek, M. P., *Topics Catal.* **3**, 289 (1996); *J. Catal.* **169**, 347 (1997).
4. Solymosi, F., Cserényi, J., and Szõke, A., *Catal. Lett.* **32**, 43 (1995); Solymosi, F., Cserényi, J., Szõke, A., Bánsági, T., and Oszkó, A., *J. Catal.* **165**, 150 (1997), and references therein.
5. Van't Blik, H. F. J., Van Zon, J. B. A. D., Huizinga, T., Vis, J. C., Köningsberger, D. C., and Prins, R., *J. Phys. Chem.* **87**, 2264 (1983).
6. Van't Blik, H. F. J., Van Zon, J. B. A. D., Huizinga, T., Vis, J. C., Köningsberger, D. C., and Prins, R., *J. Am. Chem. Soc.* **107**, 3139 (1985).
7. Solymosi, F., and Pásztor, M., *J. Phys. Chem.* **89**, 4783 (1985).
8. Solymosi, F., and Pásztor, M., *J. Phys. Chem.* **90**, 5312 (1986).
9. Basu, P., Panayotov, D., and Yates, J. T., Jr., *J. Phys. Chem.* **91**, 3133 (1987); *J. Am. Chem. Soc.* **110**, 2074 (1988).
10. Miessner, H., Gutschick, D., Ewald, H., and Müller, H., *J. Mol. Catal.* **36**, 359 (1986).
11. Wong, T. T., Stakheev, A. Yu., and Sachtler, W. H., *J. Phys. Chem.* **96**, 7733 (1992).
12. Buchanan, D. A., Hernandez, M. E., Solymosi, F., and White, J. M., *J. Catal.* **125**, 456 (1990).
13. Baumer, M., Frank, M., Libuda, J., Stempel, S., and Freund, H.-J., *Surf. Sci.* **391**, 204 (1997).
14. Evans, J., Hayden, B., Mosselmans, F., and Murray, A., *Surf. Sci.* **279**, L159 (1992).
15. Evans, J., Hayden, B., Mosselmans, F., and Murray, A., *Surf. Sci.* **301**, 61 (1994).
16. Zaki, M. I., Kunzman, G., Gates, B. C., and Knözinger, H., *J. Phys. Chem.* **91**, 1486 (1987).
17. Solymosi, F., and Knözinger, H., *J. Chem. Soc. Faraday Trans.* **86**, 389 (1990).
18. Solymosi, F., and Bánsági, T., *J. Phys. Chem.* **97**, 10133 (1993), and references therein.
19. Krause, K. R., and Schmidt, L. D., *J. Catal.* **14**, 141 (1992).
20. Solymosi, F., and Raskó, J., *J. Catal.* **115**, 107 (1989).
21. Robins, J. C., *J. Catal.* **115**, 120 (1989).
22. Mizushima, T. M., Thoji, K., and Udagawa, Y., *J. Phys. Chem.* **94**, 4980 (1990).
23. Solymosi, F., Novák, E., and Molnár, A., *J. Phys. Chem.* **94**, 7250 (1990).
24. Solymosi, F., and Bánsági, T., *J. Phys. Chem.* **96**, 1349 (1992).
25. Guczi, L., Beck, A., Zsoldos, A., and Dobos, S., *J. Mol. Catal.* **56**, 59 (1989).
26. Komiyama, M., Yamoto, K., and Ogino, Y., *J. Mol. Catal.* **56**, 78 (1989).
27. Berkó, A., Ménesi, G., and Solymosi, F., *J. Phys. Chem.* **100**, 17732 (1996).
28. Berkó, A., and Solymosi, F., *Surf. Sci. Lett.* **411**, L900 (1998).
29. Solymosi, F., Bánsági, T., and Novák, E., *J. Catal.* **112**, 183 (1988).
30. Dictor, R., and Roberts, R., *J. Phys. Chem.* **93**, 5846 (1989).
31. Krishnamurthy, R., Chuang, S. S. C., and Balakos, M. W., *J. Catal.* **157**, 512 (1995).
32. Srinivas, G., Chuang, S. S. C., and Debnath, S., *J. Catal.* **148**, 748 (1994).
33. Novák, E., Sprinceana, D., and Solymosi, F., *Appl. Catal. B.* **149**, 89 (1997).
34. Berkó, A., and Solymosi, F., *Langmuir* **12**, 1257 (1996), and references therein.
35. Norenberg, H., Tanner, R. E., Schierbaum, K. D., Fischer, S., and Briggs, G. A. D., *Surf. Sci.* **396**, 52 (1998).
36. Fischer, S., Schierbaum, K. D., and Gopel, W., *Vacuum* **48**, 601 (1997).
37. Cocks, J. D., Guo, Q., and Williams, E. M., *Surf. Sci.* **390**, 119 (1997).
38. Murray, P. W., Shen, J., Condon, N. G., Pang, S. J., and Thornton G., *Surf. Sci.* **380**, L455 (1997).

39. Szabó, A., and Engel, T., *Surf. Sci.* **329**, 241 (1995).
40. Onishi, H., and Iwasawa, Y., *Surf. Sci.* **313**, L783 (1994).
41. Poirier, G. E., Hance, B. K., and White, J. M., *J. Vac. Sci. Technol. B* **10**, 6 (1992).
42. Poirier, G. E., Hance, B. K., and White, J. M., *J. Phys. Chem.* **97**, 5965 (1993).
43. Berkó, A., Ménesi, G., and Solymosi, F., *Surf. Sci.* **372**, 202 (1997).
44. Berkó, A., and Solymosi, F., *Surf. Sci.* **400**, 281 (1998).
45. Sadeghi, H. R., and Henrich, V. E., *Appl. Surf. Sci.* **19**, 330 (1984).
46. Zhdanov, V. P., and Kasemo, B., *Surf. Sci. Rep.* **29**, 31 (1997).
47. Solymosi, F., Erdõhelyi, A., and Kocsis, M., *J. Catal.* **65**, 2351 (1980); Solymosi, F., Bánsági, T., and Erdõhelyi, A., *Trans. Faraday Soc. 1* **77**, 2645 (1981).
48. Solymosi, F., and Kiss, J., *Surf. Sci.* **149**, 17 (1985).
49. Solymosi, F., *J. Mol. Catal.* **65**, 337 (1991).